



Available online at www.sciencedirect.com

ScienceDirect

Photonics and Nanostructures – Fundamentals and Applications 16 (2015) 1–8

PHOTONICS AND
NANOSTRUCTURES
Fundamentals and Applications

www.elsevier.com/locate/photonics

Theoretical investigation of a dispersion compensating photonic crystal fiber with ultra-high dispersion coefficient and extremely low confinement loss

Jui-Ming Hsu^{*}, Wen-Hao Zheng, Cheng-Ling Lee, Jing-Shyang Horng

Department of Electro-Optical Engineering, National United University, 2, Lienda, Miaoli 36063, Taiwan, ROC

Received 26 February 2015; received in revised form 2 June 2015; accepted 5 June 2015

Available online 22 June 2015

Abstract

A dispersion compensating photonic crystal fiber (DCPCF) with ultra-high chromatic dispersion coefficient and extremely low confinement loss based on a hybrid structure of dual-concentric core photonic crystal fiber (DCC-PCF), and depressed-clad photonic crystal fiber (DeC-PCF), is theoretically investigated. To enhance the performances with regard to dispersion and confinement loss of the proposed DCPCF, a high refractive index Germanium-doped rod is introduced in the central core. For the sake of comparison, two types of DCPCF published previously were simulated simultaneously in this work. The numeric results reveal that the proposed DCPCF has a dispersion coefficient of -51625 ps/km nm and a confinement loss of $6.54 \times 10^{-4} \text{ dB/km}$ at a wavelength of $1.55 \mu\text{m}$; it undeniably has extremely good performances when compared with the other two types of DCPCF. Moreover, it is worthwhile emphasizing that the proposed structure has an advantage of easy fabrication.

© 2015 Elsevier B.V. All rights reserved.

Keywords: Dispersion compensating fiber; Photonic crystal fiber; Dispersion compensating photonic crystal fiber; Dual-concentric core fiber; Dual-concentric core photonic crystal fiber

1. Introduction

Chromatic dispersion in single mode fibers (SMFs) may induce temporal optical pulse broadening, resulting in serious restrictions in transmission data rates. Dispersion-compensating fibers (DCFs) can result in a negative dispersion coefficient, effectively compensating the positive dispersion produced by an SMF. The chromatic dispersion coefficient of conventional DCFs was approximately -100 to -250 ps/km nm [1].

Auguste et al., reported another design of DCF based on a dual-concentric core fiber (DCCF) structure with a high dispersion coefficient of -1800 ps/km nm at a wavelength of $1.558 \mu\text{m}$ [2].

Additional dispersion-compensation research involved altering the air hole size, or filling liquid in the holes of a specific layer of photonic crystal fiber (PCF), to design dual-concentric core PCFs (DCC-PCFs) [3–7]. The previous works of [3–7] are all given significant magnitude of the negative chromatic dispersion coefficient (D) to effectively compensate for the considerable positive dispersion in long distance fiber networks. Furthermore, it is well known that a larger D may decrease the length of the

* Corresponding author. Tel.: +88 637382564.
E-mail address: jmhsu@nuu.edu.tw (J.-M. Hsu).

DCF for an equivalent compensation effect, and thereby reduce the loss and nonlinear effect that resulted in the DCF.

Gerome et al., proposed a geometric DCC-PCF with a smaller-holes outer ring core (ORC) at the fourth layer; as their DCC-PCF has a chromatic dispersion of -2200 ps/km nm at a wavelength of around $1.55 \mu\text{m}$ [3]. Yu et al., filled liquid with a specific refractive index in the holes of an ORC at the fourth layer and accomplished a negative dispersion of $-19,000 \text{ ps/km nm}$ at a wavelength of around $1.55 \mu\text{m}$ [6]. We had proposed a liquid-filled hybrid structure of DCC-PCF and depressed-clad photonic crystal fiber (DeC-PCF) with an ultra-large negative dispersion coefficient of $-40,400 \text{ ps/km nm}$ at a wavelength of around $1.55 \mu\text{m}$ [7]. The design of that hybrid structure can avoid the restriction of “mutual involvement” between two supermodes, thus significantly increasing the index slope difference between the two supermodes and thereby enlarging the dispersion coefficient [7].

In this paper, to achieve an ultra-high negative dispersion, we used the hybrid of DCC-PCF and DeC-PCF [7] as a basic structure, and introduced a high refractive index Germanium-doped (Ge-doped) rod in the central core [5]. By an appropriate design, an ultra-high-dispersion DCPCF with extremely low confinement loss was finally accomplished. Furthermore, the fabrication of the proposed DCPCF is quite easy due to a fact that the hole-less ORC avoids hole collapse in the drawing process. Additionally, the proposed DCPCF is compared with Gerome’s [3] and Yu’s structures [6] for dispersion coefficient D and confinement loss (L_C).

2. Simulation models and theories

The chromatic dispersion coefficient D is used to quantify the amount of chromatic dispersion. D is defined as

$$D = \frac{-\lambda}{c} \frac{d^2 n_{\text{eff}}}{d\lambda^2}, \quad (1)$$

where λ represents the operating wavelength, c is the speed of light in a vacuum, and n_{eff} is the effective index of the fundamental guided mode in a fiber at various wavelengths.

For the sake of comparison, three types of DCPCF structure are used for simulations in this paper. Types 1 and 2 are based on the previous works of [3,6] and shown in Fig. 1(a) and (b), respectively. The proposed DCPCF described above is denoted as Type 3 and shown in Fig. 1(c). The numeric results reveal that the proposed DCPCF Type 3 has an ultra-high D and extremely low L_C when compared with DCPCF Type 1 and 2.

The theory of a DCC-PCF structure was described in detail in the previous work [3]. For clarity, it is simplistically stated as follows. In a DCC-PCF, the dual-concentric core is composed of the inner core and the ORC. The effective indices of the two supermodes, referred to as the inner and outer mode, are equal at the phase-matching wavelength λ_o . The fundamental mode coincides with the inner mode at wavelengths shorter than λ_o ; thus, the propagation field is essentially well-confined within the central core at these wavelengths, as shown in Fig. 2(a). Once the λ_o wavelength is reached, the field starts to spread out from the inner core to the

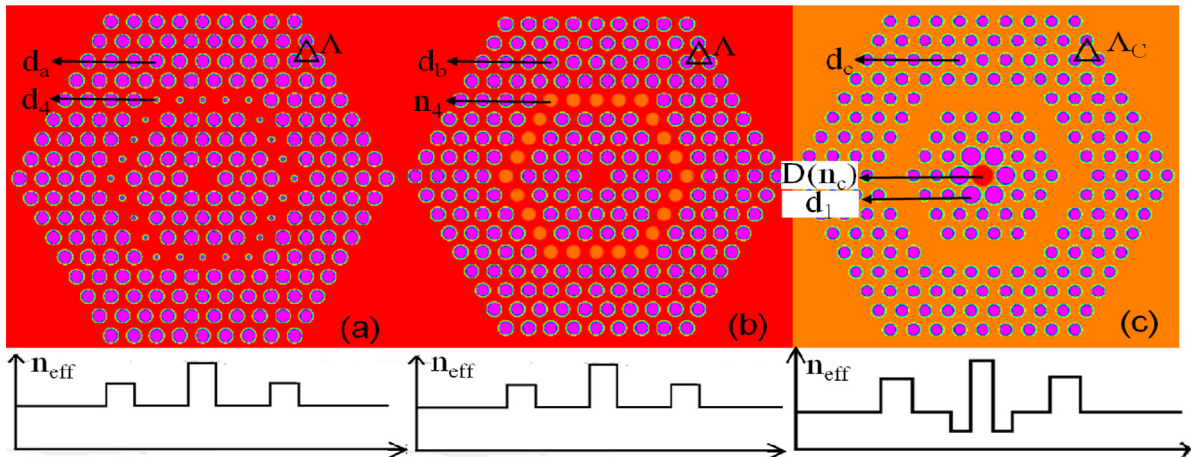


Fig. 1. Cross-sectional view and effective index profile of the DCPCFs for (a) Type 1 (the previous geometric DCC-PCF) [3], (b) Type 2 (the previous liquid-filled DCC-PCF) [6], and (c) Type 3 (the proposed DCPCF). $\Lambda = 2.300 \mu\text{m}$, $\Lambda_C = 2.100 \mu\text{m}$, $d_a = d_b = 1.400 \mu\text{m}$, $d_c = 1.150 \mu\text{m}$, $d_4 = 0.510 \mu\text{m}$, $d_1 = 1.775 \mu\text{m}$, $D = 2.000 \mu\text{m}$, $n_4 = 1.3875$, $n_c = 1.4850$. (For interpretation of the references to color in this figure legend, the reader is referred to the web version of this article.)

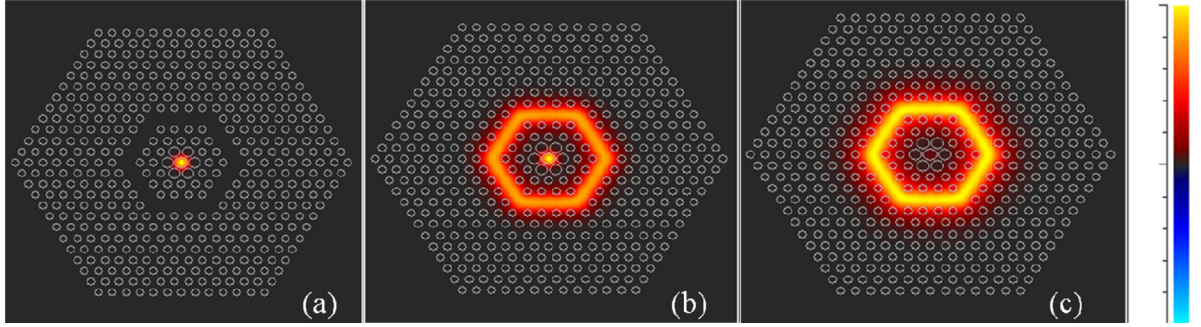


Fig. 2. Field patterns of the fundamental mode on the proposed DCPCF at a wavelength of (a) shorter than, (b) equal to and (c) longer than the phase-matching wavelength λ_o , respectively. (For interpretation of the references to color in this figure legend, the reader is referred to the web version of this article.)

ORC as indicated in Fig. 2(b). At wavelengths longer than λ_o , the fundamental mode switches to the outer mode, meaning that most of the power is effectively guided to the ORC, as shown in Fig. 2(c). According to Eq. (1), a large negative dispersion D will occur for the abruptly transitional n_{eff} at the wavelength λ_o . In other words, the larger the slope difference of index curves between the two supermodes, the larger the magnitude of the negative dispersion.

The cladding of these three types of DCPCF all consist of a triangular lattice of air holes with diameters of $d_a = d_b = 1.400 \mu\text{m}$ (Types 1 and 2), $d_c = 1.150 \mu\text{m}$ (Type 3), respectively, and pitches (center-to-center distance between the holes) of $\Lambda = 2.300 \mu\text{m}$ (Types 1 and 2), and $\Lambda_C = 2.100 \mu\text{m}$ (Type 3), in a background of undoped silica, whose refractive index can be estimated using the Sellmeier equation [8]:

$$n(\lambda) = \left[1 + \frac{0.6961663\lambda^2}{\lambda^2 - (0.0684043)^2} + \frac{0.4079426\lambda^2}{\lambda^2 - (0.1162414)^2} + \frac{0.8974794\lambda^2}{\lambda^2 - (9.896161)^2} \right]^{1/2} . \quad (2)$$

The solid cores are formed by removing a central air hole for Types 1 and 2. For DCPCF Type 1, the holes of the fourth layer – which acts as an ORC – have a smaller diameter of $d_4 = 0.510 \mu\text{m}$. Comparatively, the ORC holes for Type 2 with a diameter of d_b (the same as cladding-holes) are filled liquid with an index of $n_4 = 1.3875$. For the DCPCF Type 3, the air holes of the first layer have a larger diameter of $d_1 = 1.775 \mu\text{m}$ and the ORC is replaced by a silica-ring with a background index (without holes). For a DCCF, or a DCC-PCF, the refractive index of the inner core must be larger than that of the ORC [2]. Therefore, by an appropriate design, a Ge-doped silica rod with a higher index of $n_c = 1.4850$ and a diameter of $D = 2.000 \mu\text{m}$ is inserted into the inner core of Type 3. Gibson et al., had manufactured a photonic crystal fiber with hole-pitch (Λ) of about 120 nm, and a hole-diameter of about 60 nm [9]. Therefore, we

believe that the proposed design can be experimentally realized.

The corresponding effective index profiles of these three types of DCPCF are roughly depicted beneath the cross-sectional figures. The horizontal axes of the cross-sectional figures are the radial direction of the PCFs. The n_{eff} 's can be regarded as the weighted average of index of material filled in holes and the background (pure silica). For Fig. 1(a), the small holes at the ORC region result in a n_{eff} higher than the inner and outer cladding but lower than the inner core (which is pure silica). For Fig. 1(b), the material filled in the ORC holes has an index lower than silica (of core) but higher than air (of cladding). Therefore, for Fig. 1(a) and (b), the n_{eff} 's of the ORC regions are lower than those of the core regions but higher than those of the cladding regions. For Fig. 1(c), the ORC region is pure silica with the n_{eff} higher than those of the

inner and outer cladding. In addition, the core index of n_c is larger than the index of silica, and the first layer with large air holes has a n_{eff} lower than those of the inner and outer cladding regions.

3. Design considerations

The design is based on the previously mentioned principle: “increasing the index slope difference between two supermodes” [7]. Fig. 3 indicates the dependence of the effective indices of the inner and outer modes on the wavelength for the DCPCF Type 3 with some factor variance. The factors are held by the designed value ($\Lambda_C = 2.100 \mu\text{m}$, $d_c = 1.150 \mu\text{m}$, $d_1 = 1.775 \mu\text{m}$, $D = 2.000 \mu\text{m}$, $n_c = 1.4850$), except for the variant factor.

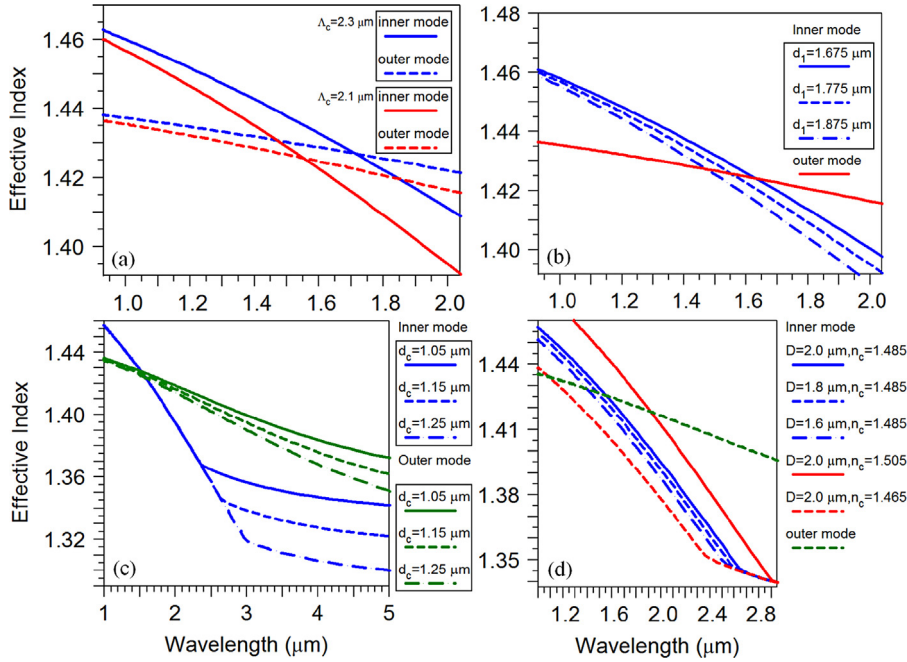


Fig. 3. Dependence of the effective indices of inner and outer modes on wavelengths for the DCPCF Type 3 with variant (a) pitch Λ_C , diameters of the holes at (b) first layer d_1 and (c) cladding d_c , (d) diameter D and index n_c of the core. (For interpretation of the references to color in this figure legend, the reader is referred to the web version of this article.)

Fig. 3(a) reveals the n_{eff} of the inner and outer modes for the proposed DCPCF with the Λ_C of 2.300 μm , and 2.100 μm , respectively. As shown in the figure, a smaller pitch causes the index curves of both the inner and outer modes with larger slopes, while the slope-variation of the inner mode is larger than that of the outer mode. Therefore, a smaller pitch results in a larger dispersion coefficient. **Fig. 3(b)** demonstrates the n_{eff} of the inner and outer modes for the proposed DCPCF where the d_1 is 1.675 μm , 1.775 μm , and 1.875 μm , respectively. The d_1 , which is the diameter of the large holes situated in the first layer of inner cladding, will not affect the outer mode, thus the index curves of the outer modes overlay with each other. As per **Fig. 3(a)**, the larger the d_1 , the larger the slope of index curve of the inner mode and the index slope difference. Therefore, a larger d_1 brings about a larger dispersion coefficient. **Fig. 3(a)** and **(b)** clarify that enlarging the cladding holes or reducing the pitch may enhance the dispersion coefficient. However, both points will thin the walls between the holes and increase the difficulty of fabrication. Therefore, the appropriate values of $\Lambda_C = 2.100 \mu\text{m}$ and $d_1 = 1.775 \mu\text{m}$ are selected in this work.

Fig. 3(c) shows the n_{eff} 's of the inner and outer modes for the proposed DCPCF with the d_c of 1.050 μm , 1.150 μm , and 1.250 μm , respectively. The index curves

of the inner modes shown in the figure reveal the characteristic of the DeC-PCF [7]. In the habitual window (C band) of the optical-fiber communications, the index curves of the inner modes overlap with each other. As shown in **Fig. 3(c)**, the larger the d_c , the larger the slope of the index curve of the outer mode, then the smaller the index slope difference. Therefore, a smaller d_c enhances the dispersion coefficient. Considering the too small cladding holes that are prone to collapse in the drawing process, thus, the proper value of $d_c = 1.150 \mu\text{m}$ is adopted in this work.

Fig. 3(d) presents the n_{eff} of the inner and outer modes for the proposed DCPCF with different factors of the inner core D , and n_c , respectively. These two factors of the inner core should not affect the outer mode, thus, the index curves of the outer modes overlay with each other for all cases. As per **Fig. 3(d)**, both D and n_c cause slight slope variations of the index curves, as they just act on shifting the index curve of the inner mode with a wavelength. In another word, varying these two parameters is almost nothing to enlarging the dispersion; nevertheless, they can be used to adjust the operation wavelength. Therefore, one can enlarge the dispersion coefficient by designing Λ_C , d_1 , and d_c , first; then use D and n_c to adjust the operation wavelength to the predetermined wavelength. According to **Fig. 3(d)**, the λ_o

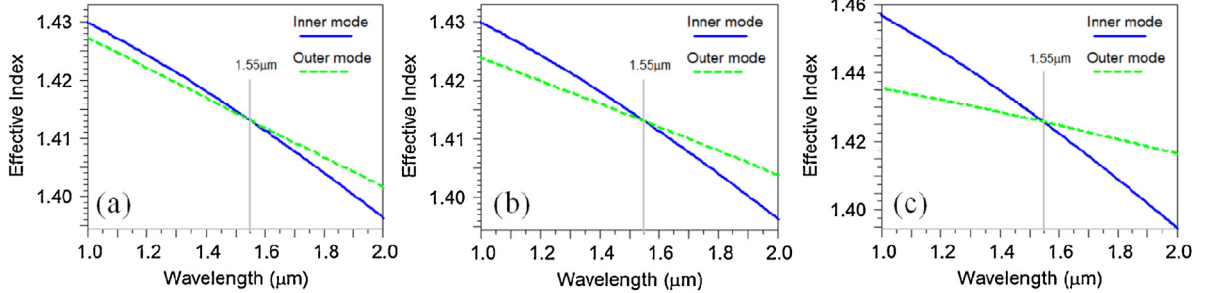


Fig. 4. The relationship between the effective indices of inner and outer modes for (1) Type 1 (the previous geometric DCC-PCF) [3], (2) Type 2 (the previous liquid-filled DCC-PCF) [6] and (3) Type 3 (the proposed DCPCF). (For interpretation of the references to color in this figure legend, the reader is referred to the web version of this article.)

shifts toward the same direction regardless of D , and n_c are either increased or decreased. In other words, the wavelength shift effects are similar between the factors of D -enlarging and n_c -enlarging. This work first set D as large as possible (2.0 μm); afterwards, n_c (1.4850) is fine tuned to situate the λ_o at a wavelength of around 1.55 μm . The advantage of this manner is keeping the doping concentration of the central rod as sparse as possible thereby reducing the material loss to the utmost level.

Considering the facile fabrication, this work leaves adequate leeway for enlarging the negative dispersion; otherwise the dispersion coefficient still has room for improvement.

4. Numeric results and discussions

4.1. Chromatic dispersions

The effective refractive index (n_{eff}) of the fundamental mode is first estimated using the plane-wave expansion method. The dispersion coefficient D is then evaluated by substituting n_{eff} into Eq. (1). Fig. 4(a)–(c), show the dependence of the effective indices of the inner and outer modes on the wavelength for the DCPCF Types 1–3, respectively. As a result of the appropriate design, the phase-matching wavelength λ_o of all the three types of the DCPCF occur approximately at 1.55 μm .

As mentioned above, the n_{eff} of a fundamental mode is equal to that of the inner mode at wavelengths of $\lambda < \lambda_o$ and agrees with that of the outer mode at wavelengths of $\lambda > \lambda_o$. Fig. 5(a) and (b) display the relation of the n_{eff} 's and the slopes of n_{eff} -curves versus the wavelength for the fundamental modes of these three types of DCPCF. Δ_1 , Δ_2 , and Δ_3 , represent the slope differences between the two supermodes of Types 1, 2, and 3, at a wavelength of around 1.55 μm , respectively. In the inner mode guiding condition ($\lambda < 1.55\text{ μm}$), the index curves in Fig. 5(a),

and the n_{eff} -slopes in Fig. 5(b) for Types 1 and 2 entirely overlap. This occurs due to the same inner structure of these two types of DCC-PCF (Fig. 1(a) and (b)). However, for the outer mode guiding condition ($\lambda > 1.55\text{ μm}$), the index curve of Type 2 is more gradual than that of Type 1 as shown in Fig. 5(a), this means that the slope of Type 2 is lower than that of Type 1 as shown in Fig. 5(b) for $\lambda > 1.55\text{ μm}$. Finally, $\Delta_2 > \Delta_1$ is realized. As mentioned above, a large slope difference results in a large negative dispersion. Therefore, the D -magnitude of Type 2 must be greater than that of Type 1 at a wavelength of around 1.55 μm .

In addition, the index-curve slopes of Type 2 and 3 are almost equal in the outer mode guiding condition ($\lambda > 1.55\text{ μm}$), as shown in Fig. 5(a), while the index curve of Type 3 is considerably steeper than that of Type 2 in the inner mode guiding condition ($\lambda < 1.55\text{ μm}$). Therefore, as shown in Fig. 5(b), $\Delta_3 > \Delta_2$ results in a larger D -magnitude of Type 3 when compared with that of Type 2 at a wavelength of around 1.55 μm .

Accordingly, one can deduce that the proposed DCPCF (Type 3) has the largest D -magnitude, and that of the DCC-PCF Type 2 and 1 are medium, and smallest, respectively.

Fig. 6 shows the dependence of the estimated chromatic dispersion coefficient D on a wavelength for the three types of DCPCF. In Fig. 6, Types 1–3, have a minimum chromatic dispersion of -2162 , -18597 , and -51625 ps/km nm at a wavelength of around 1.55 μm , respectively. As per our expectations, the numeric results indicated in Fig. 6 absolutely fit in with the anticipation in the preceding paragraph.

4.2. Optical losses

4.2.1. Confinement losses (L_C)

The loss is another important issue for the DCFs. The confinement loss (L_C) for each structure can be deduced

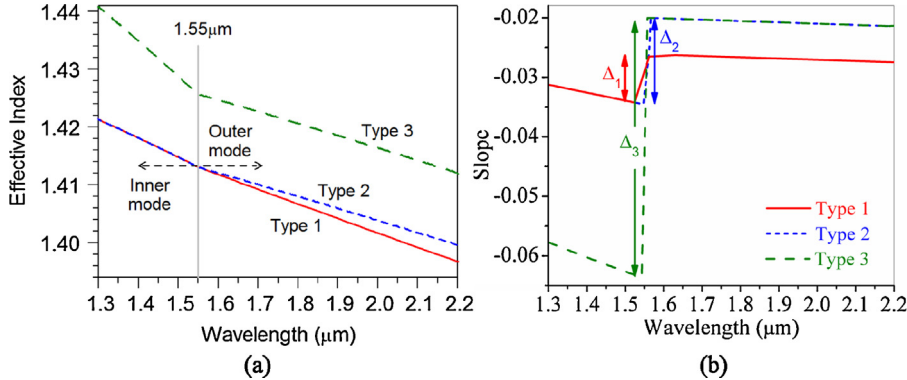


Fig. 5. Relation of (a) the effective indices and (b) the slopes of n_{eff} -curves versus wavelengths for the fundamental modes of three types of DCPCF. The phase-matching wavelength λ_o are all designed to locate at a wavelength of around 1.55 μm. (For interpretation of the references to color in this figure legend, the reader is referred to the web version of this article.)

by the value of the imaginary part of effective indices (n_{eff}) as

$$L_C = 8.686 \times k_o \times \text{Im}[n_{\text{eff}}], \quad (3)$$

where k_o is the wave number in free space, and $\text{Im}[n_{\text{eff}}]$ represents the imaginary part of n_{eff} .

As is widely known, the higher index of the central core must confine the greater part of energy in the inner core. Therefore, it is reasonable to anticipate that the proposed DCPCF has a considerably lower confinement loss. To verify this anticipation, the numeric results of the L_C for the three types of DCPCF were estimated by using Eq. (3) and listed in Table 1. As shown in the table, the confinement losses of these three types of DCPCF are quite small. In particular, the confinement loss of the proposed DCPCF Type 3 is extremely low (6.54×10^{-4} dB/km).

Table 1

Confinement losses for the three types of DCPCF at a wavelength of around 1.55 μm.

	DCPCFs		
	Type 1	Type 2	Type 3
Confinement loss (dB/km)	1.58×10^{-3}	2.86	6.54×10^{-4}

4.2.2. Absorption losses (L_A)

A drawback of increasing the core index is increased absorption loss due to the higher GeO₂ doping. The absorption loss L_A including Rayleigh scattering and infrared absorption in a fiber is given by [10]:

$$L_A = \frac{1}{\lambda^4} \frac{\int A(r) P(r) r dr}{\int P(r) r dr} + 6.65 \times 10^{12} \exp\left(-\frac{52.62}{\lambda}\right), \quad (4)$$

where λ , in μm, is the wavelength in a vacuum, $P(r)$ and $A(r)$, respectively, represent the light intensity and Rayleigh scattering coefficient in the radial distance r . The relative-index difference dependence of Rayleigh scattering coefficient for a GeO₂-doped glass is given by [10]

$$A = A_o (1 + 0.44\Delta) \quad (5)$$

where $A_o = 0.8$ (dB/km) μm⁴ is the Rayleigh scattering coefficient of pure silica glass, $\Delta = (n_c - n_{\text{SiO}_2})/n_{\text{SiO}_2}$, in %, the relative-index difference of the GeO₂-doped glass. For a GeO₂-doped core with step-index profile and a refractive index of $n_c = 1.4850$, the Eq. (4) can be rewritten as

$$L_A = \frac{1.8}{\lambda^4} + 6.65 \times 10^{12} \exp\left(-\frac{52.62}{\lambda}\right). \quad (6)$$

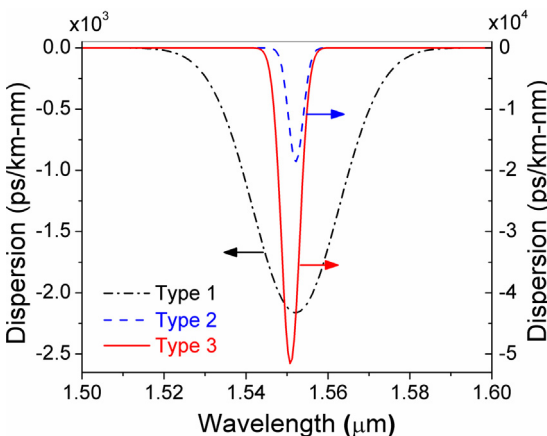


Fig. 6. Relation of the chromatic dispersion coefficient versus wavelengths for the three types of DCPCF. (For interpretation of the references to color in this figure legend, the reader is referred to the web version of this article.)

In addition, the absorption loss of a pure silica glass can be expressed as

$$L_A = \frac{0.8}{\lambda^4} + 6.65 \times 10^{12} \exp\left(-\frac{52.62}{\lambda}\right). \quad (7)$$

According to Eq. (6) and (7), at a wavelength of $1.55 \mu\text{m}$, the absorption losses of a pure silica glass, and a GeO_2 -doped rod used in this work, are 0.1506 dB/km and 0.3237 dB/km , respectively.

4.2.3. Total losses (L_T)

Consequently, the total loss is the sum of the confinement loss L_C and absorption loss L_A . Assuming that L_{T1} , L_{T2} , and L_{T3} , respectively, represent the total losses of DCPCF Type 1, Type 2, and Type 3, thus $L_{T1} = 0.152 \text{ dB/km}$, $L_{T2} = 2.86 \text{ dB/km} + L_{A2}$ (L_{A2} represent the absorption loss of DCPCF Type 2), and $L_{T3} = 0.324 \text{ dB/km}$ at a wavelength of $1.55 \mu\text{m}$. The total loss of the proposed DCPCF L_{T3} is significantly smaller than L_{T2} , while slightly larger than L_{T1} .

Fortunately, the proposed DCPCF possesses an extremely high negative chromatic dispersion value; the compensation length is accordingly reduced as is the accumulative attenuation. For example, the transmission fiber of a standard SMF, which has a chromatic dispersion $D_{TF} \cong +17 \text{ ns/km nm}$ at a wavelength of $1.55 \mu\text{m}$, spans the length (L_{TF}) of 40 km . According to the compensation condition: $D_{TF}L_{TF} + D_{DCF}L_{DCF} = 0$, the DCPCF Type 1 and Type 3 need the lengths of $L_{DCF1} \cong 314.5 \text{ m}$ and $L_{DCF3} \cong 13.2 \text{ m}$, respectively, to compensate the dispersion of the transmission fiber at a wavelength of $1.55 \mu\text{m}$. Eventually, throughout the compensation length, the accumulative attenuations of DCPCF Type 1 and Type 3 are about 0.048 dB and 0.004 dB , respectively. Therefore, the accumulative attenuation of the proposed DCPCF is smaller than that of the DCPCF Type 1 yet.

5. Fabricating considerations

Like as the fabrication process of general PCF, the proposed DCPCF can be easily fabricated by using the stack-and-draw method. The PCF preform is realized by stacking a number of capillary silica tubes and rods with the same outer diameter, while the different inner diameters (for tubes) will form the desired air–silica structure. The central rod is Ge-doped in the center which is just like a traditional MCVD fiber. The ORC at the fourth layer is stacked by using 24 rods of undoped silica. After the stacking process, the capillaries and rods are held together, and a DCPCF, as shown in Fig. 1(c), is then

accomplished through the intermediate drawing and final drawing process.

When compared with the other two types of DCC-PCF, our proposed DCPCF Type 3 is extremely easy to fabricate. For the DCC-PCF Type 1, the ORC is composed of 24 capillaries with a small inner diameter of $d_4 = 0.51 \mu\text{m}$. The holes of the ORC are so small that they are very easy to collapse in the drawing process. To maintain a perfect structure of the PCF, even more careful control of the drawing process is necessary. A lower temperature level, a slight overpressure inside the pre-form, and a proper drawing-speed adjustment are helpful to the drawing process [11]. However, since the holes of the ORC are so small, they are prone to collapse even though the drawing process is carefully controlled.

For the DCC-PCF Type 2, the diameter of the holes at the ORC is identical to that of the cladding holes, while the ORC holes must be filled with liquid throughout the whole length of a PCF. For selectively filling the holes with liquid in a PCF, some practical techniques had been proposed, but not that many. For a hollow core PCF (HC-PCF), a hollow-core fiber (HCF) is spliced to the HC-PCF using a fusion splicer; the hole of the HCF is aligned to the central hole of the HC-PCF, and the solid cladding of the HCF seals the cladding holes of the HC-PCF [12]. To selectively fuse the outer rings of the HC-PCF, the fusion splicing technique with tailored electric arc energies and fusion times is used [13]. Utilizing the different flow speed of the liquid for various sizes of air holes to selectively fill the holes with liquid [14,15]. A more precise control can be achieved by selectively blocking the unwanted air holes by sealing with epoxy, so that only the open air-holes can be filled with polymer [16]. The roughly selective liquid-filling techniques [12–15] are not suitable for the ORC in the DCPCFs. Kerbage et al., proposed a precise control technique for filling specific holes with liquid [16]. However, the holes of their fiber have a diameter of up to $40 \mu\text{m}$.

It is directly perceived through the senses that drawing the PCF with tiny ORC-holes without collapse (Type 1) or filling liquid into several dozen meter lengths of capillaries with a diameter of μm -scale (Type 2) are fairly difficult. Comparatively, the fabrication process of the DCPCF Type 3 is considerably simpler since its ORC is just a ring of solid silica without holes.

6. Conclusions

This work theoretically investigated a DCPCF with ultra-high chromatic dispersion and extremely low confinement loss, by introducing a high refractive index Germanium-doped rod into the central core

of the PCF, based on a hybrid structure of DCC-PCF and DeC-PCF. When compared with previous studies, it has been verified that the dispersion coefficient of the proposed DCPCF is certainly high ($D = -51625 \text{ ps/km nm}$), and the confinement loss is really low ($L_C = 6.54 \times 10^{-4} \text{ dB/km}$), at a wavelength of $1.55 \mu\text{m}$. Furthermore, it is worthwhile emphasizing that the hole-less ORC structure of the proposed DCPCF proposes a simpler fabrication process.

References

- [1] A.M. Vengsarkar, W.A. Reed, Dispersion-compensating single-mode fibers: efficient designs for first- and second-order compensation, *Opt. Lett.* 18 (1993) 924–926.
- [2] J.L. Auguste, J.-M. Blondy, J. Maury, B. Dussardier, G. Monnom, R. Jindal, K. Thyagarajan, B.P. Pal, Conception, realization, and characterization of a very high negative chromatic dispersion fiber, *Opt. Fiber Technol.* 8 (2002) 89–105.
- [3] F. Gerome, J.L. Auguste, J.M. Blondy, Design of dispersion-compensating fibers based on a dual-concentric-core photonic crystal fiber, *Opt. Lett.* 29 (2004) 2725–2727.
- [4] X. Zhao, G. Zhou, S. Li, Z. Liu, D. Wei, Z. Hou, L. Hou, Photonic crystal fiber for dispersion compensation, *Appl. Opt.* 47 (2008) 5190–5196.
- [5] S. Yang, Y. Zhang, X. Peng, Y. Lu, S. Xie, J. Li, W. Chen, Z. Jiang, J. Peng, H. Li, Theoretical study and experimental fabrication of high negative dispersion photonic crystal fiber with large area mode field, *Opt. Express* 14 (2006) 3015–3023.
- [6] C.P. Yu, J.H. Liou, S.S. Huang, H.C. Chang, Tunable dual-core liquid-filled photonic crystal fibers for dispersion compensation, *Opt. Express* 16 (2008) 4443–4451.
- [7] J.M. Hsu, G.S. Ye, Dispersion ultra-strong compensating fiber based on a liquid-filled hybrid structure of dual-concentric core and depressed-clad photonic crystal fiber, *J. Opt. Soc. Am., B* 29 (2012) 2021–2028.
- [8] I.H. Malitson, Interspecimen comparison of the refractive index of fused silica, *J. Opt. Soc. Am.* 55 (1965) 1205–1209.
- [9] B.C. Gibson, S.T. Huntington, S. Rubanov, P. Olivero, Exposure and characterization of nano-structured hole arrays in tapered photonic crystal fibers using a combined FIB/SEM technique, *Opt. Express* 13 (2005) 9023–9028.
- [10] M. Ohashi, K. Shiraki, K. Tajima, Optical loss property of silicon-based single mode fibers, *J. Lightwave Technol.* 10 (1992) 539–543.
- [11] F. Poli, A. Cucinotta, S. Selleri, *Photonic Crystal Fibers Properties and Applications*, Springer, Dordrecht, Netherlands, 2007.
- [12] C. Martelli, J. Canning, K. Lyttikainen, N. Groothoff, Water-core fresnel fiber, *Opt. Express* 13 (2005) 3890–3895.
- [13] L. Xiao, W. Jin, M.S. Demokan, H.L. Ho, Y.L. Hoo, C. Zhao, Fabrication of selective injection microstructured optical fibers with a conventional fusion splicer, *Opt. Express* 13 (2005) 9014–9022.
- [14] Y. Huang, Y. Xu, A. Yariv, Fabrication of functional microstructured optical fibers through a selective-filling technique, *Appl. Phys. Lett.* 85 (2004) 5182–5184.
- [15] K. Nielsen, D. Noordegraaf, T. Srensen, A. Bjarklev, T.P. Hansen, Selective filling of photonic crystal fibres, *J. Opt., A: Pure Appl. Opt.* 7 (2005) L13–L20.
- [16] C. Kerbage, B.J. Eggleton, Numerical analysis and experimental design of tunable birefringence in microstructured optical fiber, *Opt. Express* 10 (2002) 246–255.